



AN EXPERIMENTAL STUDY ON STEEL PIPE CONCRETE COMPOSITE BRIDGE PIER

Masaki MINAKAWA¹, Hirokazu KUNIMATSU², Kenji IKEDA³,
Hiroshi MIKAMI⁴ and Norimitsu KISHI⁵

SUMMARY

This study focuses on a composite bridge pier using steel pipes, which has a high load bearing capacity and is expected to contribute to labor-saving and the reduction of construction periods and costs because of its simple structure. This bridge pier has steel pipes with outer ribs in the bridge pier section in place of axial rebars. Large-scale wall-type pier models of RC and composite structures were constructed to be a one-third scale of the actual pier, and lateral cyclic loading tests were conducted to compare their load bearing capacity. As a result, the composite bridge pier using steel pipes had load bearing capacity, toughness and energy absorption power that were more than or equal to those of the RC structure. It was also revealed that, because steel pipes bore most of the shearing force at the base of the pier, the tension shared by the stirrups and tie-bars was low and the extent of damage to the base was less than that of a ferroconcrete bridge pier.

1. INTRODUCTION

In Japan, proposed cost reduction of infrastructure development has further intensified in recent years, and labor-saving construction and reduction of construction period are also demanded due to the shortage and aging of technical workers. At the same time, improvement in earthquake-proof performance of piers and other important structures has been strongly demanded since the Hyogo-ken Nambu Earthquake of 1995.

The composite bridge pier incorporating steel pipes (SRC) was invented as a structure to contribute to the reduction of construction costs of low or medium-level piers approximately 30 m in height. It is characterized by the placement of steel pipes with outer ribs that adhere excellently to concrete, together with axial rebars in the cross section of the pier. Since most axial rebars can be replaced by steel pipes, it is a structure that enables reduced reinforcement and labor-saving construction, therefore reduced work hours and construction cost can be expected. Figure 1 shows a conceptual drawing of the composite

¹ Senior researcher, Structures Division, CERl of Hokkaido, Sapporo, Japan. Email: 86164@ceri.go.jp

² Researcher, Structures Division, CERl of Hokkaido, Sapporo, Japan. Email: h-kunimatsu@ceri.go.jp

³ Director, Structures Division, CERl of Hokkaido, Sapporo, Japan. Email: ikedak@ceri.go.jp

⁴ Director, Sumitomo Mitsui Construction Co., Ltd. Nagareyama, Japan.

⁵ Professor, Muroran Institute of Technology, Muroran, Japan.

bridge pier using steel pipes pier and Photograph 1 shows a steel pipe with outer ribs.

In past studies [1-3], it was confirmed that this structure has a load bearing capacity equal to or higher than that of conventional reinforced concrete structure (RC) piers and that it is extremely tough in experiments using small specimens with an aspect ratio of 1:2.5 or less of the pier.

There are, however, many matters that must be clarified including the burden of the shearing force of steel pipes, stress-sharing properties on the wide side of the cross section and the effects of stirrups and tie-bars, when applying this structure to a wall-type pier structure (aspect ratio is 1:2.5 or more), which is widely used for bridges in general.

In this study, therefore, a large scale wall-type pier specimens with RC and SRC structures were produced on a scale of approximately 1/3 of an actual bridge with an aspect ratio of 1:3 or more, a long-side length of 2.5 m and a pier height of 3.5 m, and lateral cyclic loading tests were conducted [4, 5] to compare the load bearing capacity.

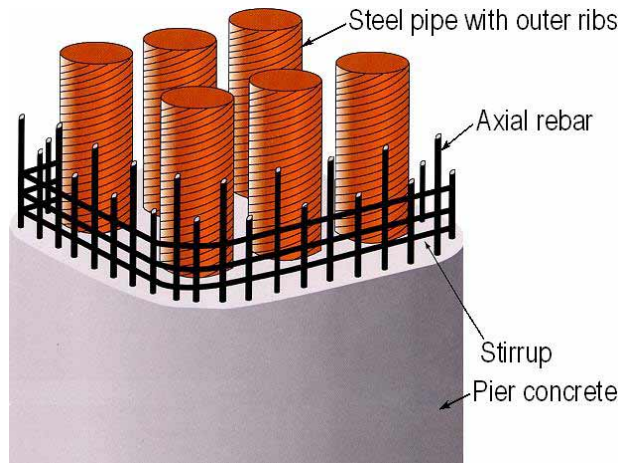


Fig.1 Composite bridge pier using steel pipes



Photo.1 Steel pipe with outer ribs

2. EXPERIMENTAL OVERVIEW

2.1 Outline of specimens

Figure 2 shows an overview of the specimens and a measurement location map. Two types of specimen were used for this experiment – an RC structure specimen and an SRC structure specimen, which has three steel pipes with outer ribs (outer diameter: 500 mm, thickness: 6 mm) placed in a line.

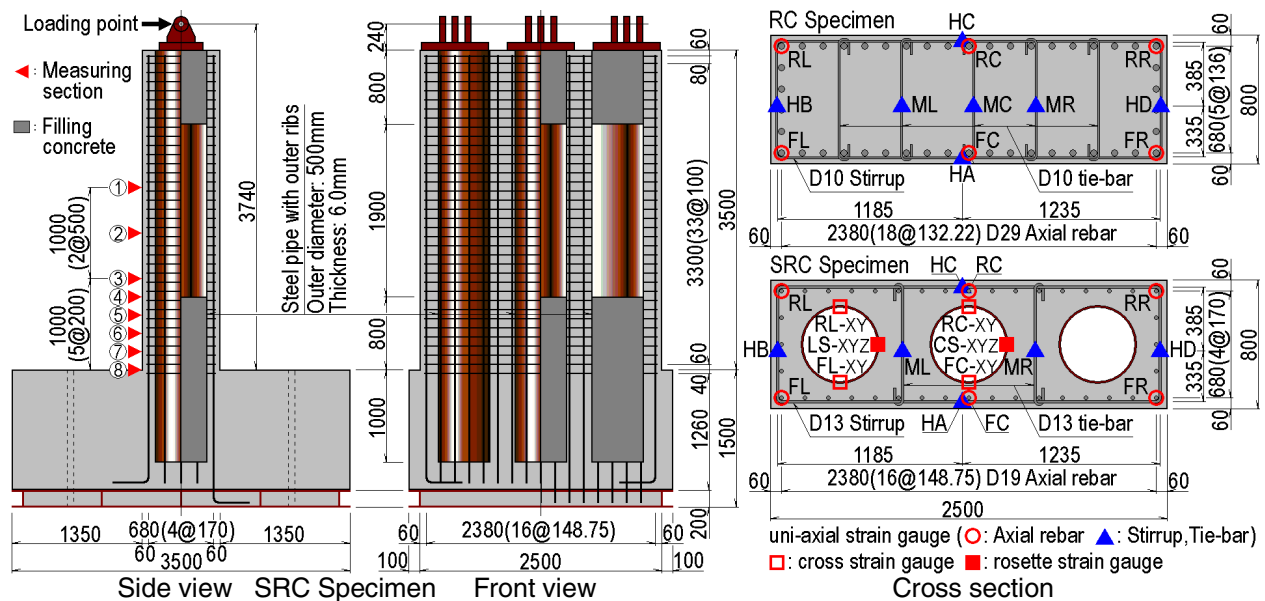


Fig.2 Outline of specimens and measuring points (unit: mm)

The section size of specimens was 800 mm in small side length, 2,500 mm in long side length, 1:3.125 in aspect ratio and 3,500 mm in specimen height. Reinforcement of the two specimens was arranged to make the conversion stirrup ratio 0.2% using D29 (RC) and D19 (SRC) for axial rebars and D10 (RC) and D13 (SRC) for stirrups and tie-bars. Steel pipes were filled with concrete up to 1D (small side width: 800 mm) from the base and 1D at the top.

Bar arrangement and other plans for the two specimens were prepared in accordance with the Specification of Japan Highway Bridge Manual, and the design was conducted by the multi-section method [6] using standard values for the materials, so that the two specimens would have almost equal bending capacity. Table 1 shows the mechanical properties of the steel materials and concrete used.

Table 1 Mechanical properties of steels and concretes

Steels		RC Specimen		SRC Specimen	
		Yield strength	Tensile strength	Yield strength	Tensile strength
Steel pipe (SKK490)		-	-	478.0 MPa	627.0 MPa
Stirrup and tie-bar (SD295A)	D10	375.1 MPa	588.7 MPa	-	-
	D13	-	-	377.2 MPa	559.5 MPa
Axial rebar (SD345)	D19	-	-	383.3 MPa	590.4 MPa
	D29	373.6 MPa	602.7 MPa	-	-

Concretes		RC Specimen	SRC Specimen
Age of test		34 days	29 days
Compressive strength		31.0 MPa	31.0 MPa
Young's modulus		19.9 GPa	32.3 GPa
Poisson's ratio		0.217	0.210

Photograph 2 shows the shape of a steel pipe with outer ribs. A standardized steel pipe with outer ribs has spiral-shaped ribs with a height of 2.5 mm, crest width of 4.0 mm and intervals of 40 mm as shown in Photograph 1. In this study, however, ribs of 6.0 mm in height and 9.0 mm in crest width were welded on plain steel pipes at intervals of 80 mm to achieve an equal adhesion effect, due to the difficulty of obtaining materials. Steel pipes with outer ribs were fixed by burying a length twice the pipe diameter into the footing.



Photo.2 Shape of steel pipe with outer ribs

2.2 Outline of loading tests

Figure 3 shows a schematic diagram of the experimental setup. In the experiment, each specimen was placed at a medium pier of a full-size two-span continuous beam, 32 m in total length, 30 m in span length and 1,010 kN in total weight, the superstructure and specimens were joined with a pin, and a hydraulic jack was installed at the pinned part to apply load.

The height from the crest of the specimen to the center of the pin was 240 mm, and the height from the crest of the footing to the loading point was 3,740 mm. Also, weight was adjusted by placing steel plates on the beam directly above the specimen to make the dead load of the superstructure applied to the specimen approximately 980 kN (the axial stress applied in a vertical direction to the specimen was 0.49 MPa as a high pier was not taken into consideration). The applied load was measured using load cells, and the horizontal displacement at each point was measured with built-in reel type displacement transducers.

Loading was repeated three times each by gradually changing the displacement until the ultimate state was reached, with displacement control using multiples (e.g., $2 \delta_y$, $3 \delta_y$) of the yield-displacement δ as amplitudes. The yield-displacement of the SRC specimen was the displacement at the time when either axial rebars or steel pipes reached the yield strain. Photograph 3 shows a scene of the loading test.

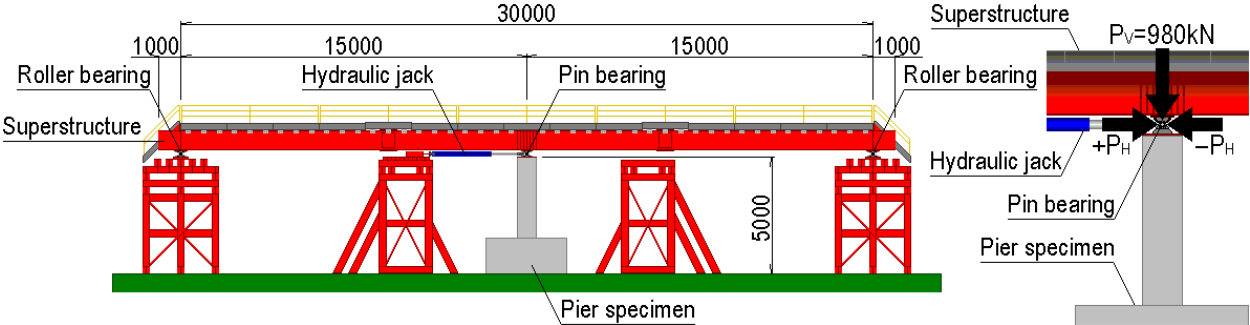


Fig.3 Experimental setup (unit: mm)



Photo.3 Scene of loading test

3. EXPERIMENTAL RESULTS AND DISCUSSIONS

3.1 Hysteretic loop of load-displacement

Figure 4 shows the hysteretic loop of load-displacement of the two specimens. Table 2 shows a comparison of experiment and calculation results. Calculation values were found by the multi-section method using the material testing results.

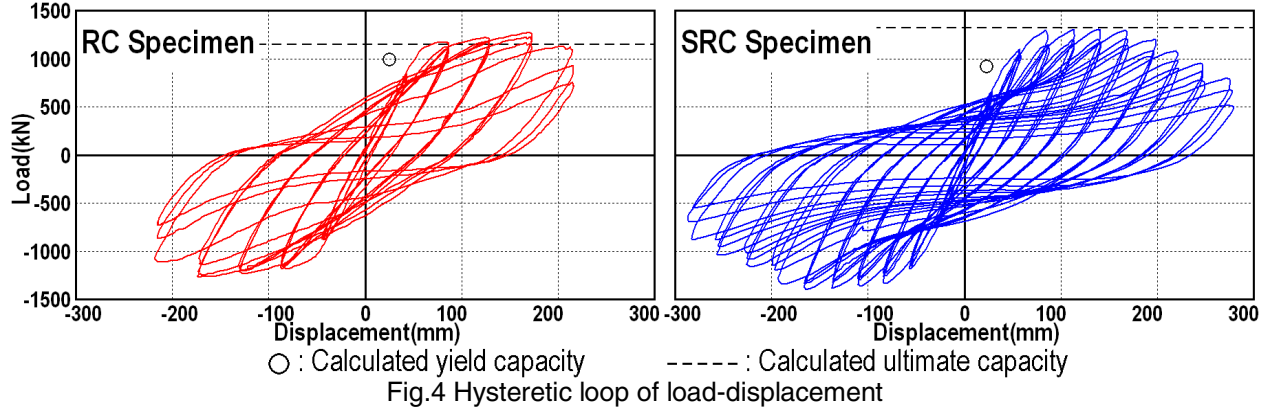


Table 2 List of both experimental and analytical results

Specimen		RC Specimen		SRC Specimen	
		Yield point	Ultimate state	Yield point	Ultimate state
Experiment	Capacity (kN)	836.8	1,241.0	644.9	1,307.3
	Displacement (mm)	42.9	215.0	27.5	275.4
Calculate	Capacity (kN)	986.5	1,145.4	920.5	1,321.2
	Displacement (mm)	25.0	321.0	23.0	192.3

In the case of the RC specimen, axial rebars yielded at 840 kN, the load increased gradually to $2-4 \delta_y$ and a maximum load of 1,241 kN was reached at $4 \delta_y$. The test was then finished because the load decreased with the breakage of axial rebars and fell below the yield load at $6 \delta_y$.

In the case of the SRC specimen, axial rebars yielded at 645kN and almost reached the maximum capacity at $3 \delta_y$. Displacement was then increased to $6 \delta_y$ while retaining the capacity. Exfoliation of cover concrete at the bottom began at $6 \delta_y$, and the capacity gradually decreased after that with the progress of exfoliation and breaking of axial rebars. The test was finished when the value fell far short of the yield load at the third loading of $10 \delta_y$. The maximum load was 1,307 kN at $5 \delta_y$.

Compared with the SRC specimen, the increase in load after δ_y was smaller for the RC specimen. This was because the maximum capacity was almost reached with the yield of the outermost axial rebars (at δ_y) in the case of the RC specimen, while a further gradual yield occurred from the outer end of steel pipes after the yield of axial rebars in the case of the SRC specimen. Also, the decrease in load by breaking of the axial rebars was more rapid in the RC specimen than in the SRC specimen. This was also because most of the RC specimen capacity was borne by the outermost axial rebars.

Figure 5 shows a comparison of load-displacement envelopes of the two specimens. The figure normalizes the horizontal axis with δ_y . From the figure, it can be seen that the section where the maximum capacity was maintained was longer in the SRC specimen than in the RC specimen, and that a large ductility factor was found without a dramatic decrease in capacity even after the maximum capacity.

This means that the SRC structure has greater earthquake-proof performance than the RC structure.

3.2 Size of the damaged area

Figure 6 shows the distribution of longitudinal strain of axial rebars and steel pipes, which was classified to study the damaged area (plastic hinge area) of the SRC structure in a wall-type pier.

In the case of the RC specimen, three of the outermost axial rebars, which had come under tension when load was applied on the positive side, were chosen and their data were schematized. For the SRC specimen, tensile strain on both ends of steel pipes were schematized. Strain values of up to $4 \delta_y$ and $6 \delta_y$ were plotted for axial rebars and steel pipes, respectively, because the values of the strain gauge that could not be measured increased dramatically after $4-6 \delta_y$ in both cases. In the figure, the values of the strain gauge that could not be measured due to breaking of the gauge itself or other reasons are shown as zero.

In the case of the RC specimen, the strain of axial rebars increased dramatically up to approximately 400 mm above the basement at $2 \delta_y$, and 1,000 mm above the basement at $4 \delta_y$, and discontinuity of the strain became remarkable. This means that the damaged area expanded with an increase in the displacement amplitude.

In the case of the SRC specimen, on the other hand, the strain distribution of steel pipes was discontinuous up to approximately 600 mm above the basement at $4 \delta_y$ and 800 mm above the basement at $6 \delta_y$, indicating that the heavily damaged area was smaller compared with the RC specimen.

3.3 Strain distribution of stirrups and tie-bars

Figure 7 shows the strain distribution of stirrups and tie-bars that are placed in the direction of the pressurized axis. The figure shows the distribution in the column height direction when the displacement amplitude was $2 \delta_y$, $4 \delta_y$ and the maximum. Strain values were measured at 5 points (HB, HD, ML, MC and MR) of each section of the RC specimen, and 4 points (HB, HD, ML and MR) of the SRC specimen. All the strain values of both positive and negative sides were schematized.

From the results of $2 \delta_y$ loading, it can be seen that strain of stirrups at the end of the RC specimen was several times as large as that of the SRC specimen, up to the height of approximately 1,000 mm above the basement. At the time of $4 \delta_y$ loading, on the other hand, it can be seen that yield strain was still not

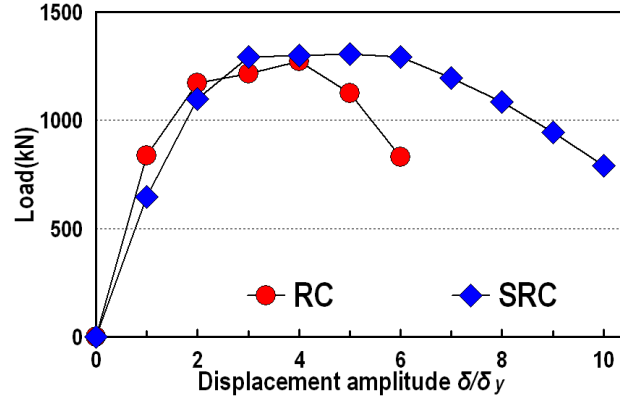


Fig.5 Comparison of load-displacement envelope

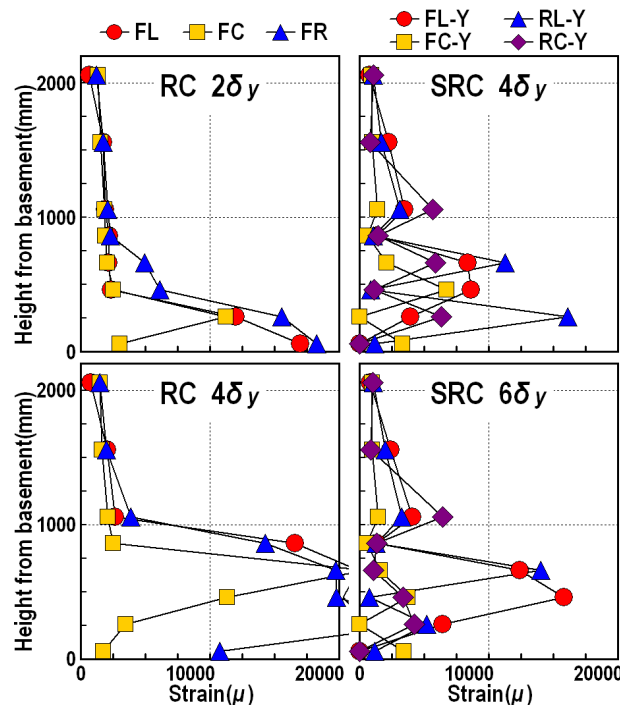


Fig.6 Strain distribution of axial rebars and steel pipes

reached at 1,000 μ or lower for the SRC specimen, although values higher than yield strain were found in some stirrups of the specimen. The strain level of the SRC specimen at the maximum displacement amplitude was 4 δ_y and it was not significantly different from that at the time of loading. Measurement was impossible for several stirrups in the RC specimen and the strain distribution properties varied greatly.

Stirrups and tie-bars in the direction of the pressurized axis had a function of restricting expansion of concrete during large deformation and greatly affect toughness of columns. Compared with the RC specimen, strain values of the SRC specimen were small at all displacement amplitudes and did not even reach the yield strain (approximately 1,800 μ).

It can thus be seen that the shared strain of stirrups and tie-bars at the bottom of the pier was large in the case of the RC structure and small in the case of the SRC structure, and that the shearing burden on stirrups became smaller in the SRC structure. This is thought to be because steel pipes bore a great deal of shearing force and reduce the shearing force applied to the RC part outside the steel pipes in the case of the SRC structure.

3.4 Maximum shear stress of steel pipes

Figure 8 shows the maximum shear stress that was applied to steel pipes of different measurement heights for each displacement amplitude, based on the measurement results of rosette strain gauges placed at the measuring points CS and LS at the center of the steel pipe section of the SRC specimen. The maximum shear stress τ_{max} was found by Equation (1).

$$\tau_{max} = \frac{E}{2(1+\nu)} \cdot \gamma_{max} \quad (1)$$

$$\gamma_{max} = \sqrt{2\{(\varepsilon_a - \varepsilon_b)^2 + (\varepsilon_b - \varepsilon_c)^2\}} \quad (2)$$

Where, γ_{max} : maximum shear strain, ε_a : longitudinal strain, ε_b : strain in the 45 degree declined direction from ε_a and ε_c , ε_c : circumferential strain, E : Young's modulus (206 GPa) and ν : Poison's ratio (0.3).

While τ_{max} at 200 mm above the basement was not

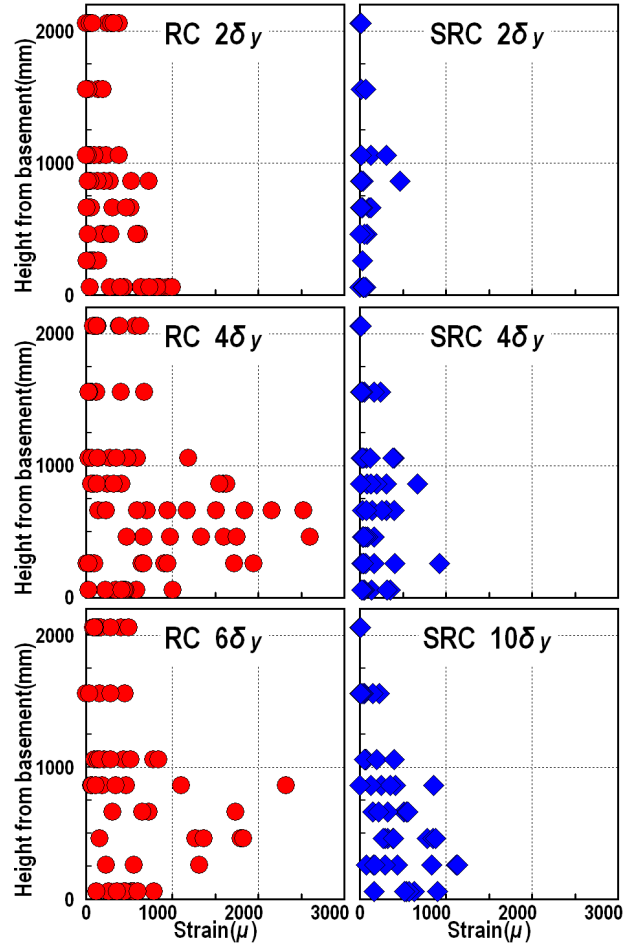


Fig.7 Strain distribution of stirrups and tie-bars

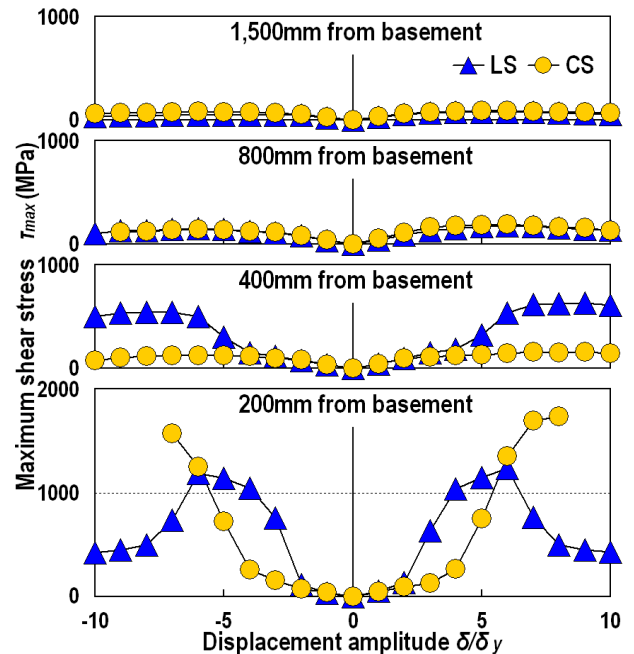


Fig.8 Maximum shear stress of steel pipes

plotted because it increased hyperbolically with an increase in the displacement amplitude at both LS and CS, and measurement with the strain gauge became impossible at $+8 \delta_y$ or after for steel pipes at the center (CS), it was presumed that shear stress tended to increase maximally. The maximum value was approximately 1,700 MPa at the time of $+8 \delta_y$ loading. The maximum value for steel pipes at the end (LS) was approximately 1,200 MPa at the time of $6 \delta_y$ loading, and τ_{max} decreased dramatically after that with an increase in displacement amplitude.

As τ_{max} at 400 mm above the basement began to differ between the steel pipes at the center and the end from approximately $5 \delta_y$, it can be seen that a larger shearing force was borne by the steel pipes at the end than those at the center. While shear stress tended to increase with an increase in displacement amplitude for both steel pipes, the maximum value was seen at the time of $7-9 \delta_y$ and decreased with an increase in displacement amplitude after that. At 400 mm above the basement, τ_{max} was 120 to 150 MPa for steel pipes at the center and 530 to 630 MPa for pipes at the end.

For both steel pipes, the relationship between the displacement amplitude and τ_{max} was almost the same at 800 and 1,500 mm above the basement. At 800 mm above the basement, τ_{max} was far lower than the stress levels at 200 and 400 mm above the basement, and it was 150 to 190 MPa at the maximum. The level of τ_{max} was even lower at 1,500 mm above the basement and was 50 to 90 MPa at the maximum.

It can thus be seen that the maximum shear stress share of steel pipes was extremely large in an area up to 200 mm above the basement and a large shearing force is borne by steel pipes around the bottom of the pier. It is therefore presumed that the tension shared by stirrups and tie-bars in this area would become far smaller than that in the case of the RC structure, as mentioned in 3.3.

3.5 Equivalent viscous damping factor

To evaluate the energy absorption capacity and damping of the SRC structure, the equivalent viscous damping factor was studied. The equivalent viscous damping factor h_{eq} can be expressed by the schema in Figure 9 and Equation (3) [6].

$$h_{eq} = \frac{1}{2\pi} \frac{\Delta W}{W} \quad (3)$$

Where, W : elastic strain energy of the pier by equivalent stiffness and the area of the triangle shown in Figure 9 (kNm) and ΔW : the total amount of energy absorbed by the pier per cycle and the area of hysteretic loop of load-displacement (kNm) shown in Figure 9.

Figure 10 shows the relationship between the displacement amplitude and the equivalent viscous damping factor of the two specimens. In the case of the RC specimen, h_{eq} increased proportionally with an increase in displacement amplitude and reached the maximum value of 0.23 at $4 \delta_y$.

In the case of the SRC specimen, on the other hand, the tendency of h_{eq} to increase to a displacement

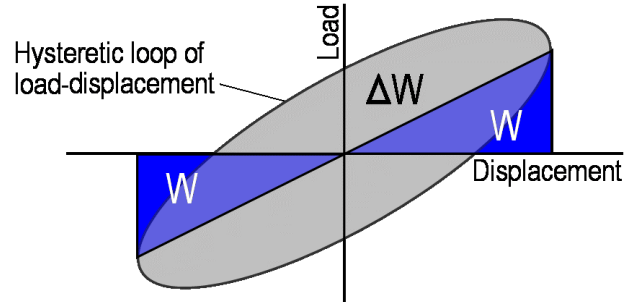


Fig.9 Equivalent viscous damping factor

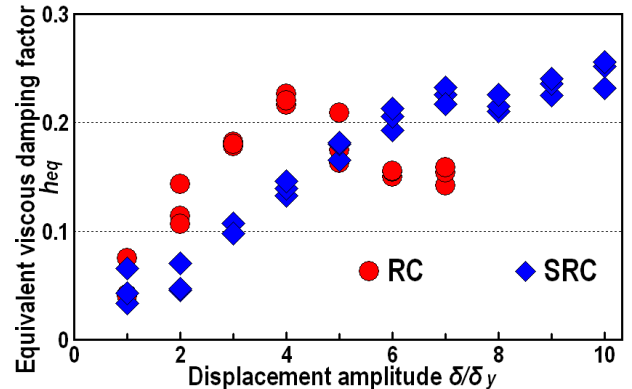


Fig.10 Comparison of equivalent viscous damping factor

area as large as $10 \delta_y$ did not change although the gradient of increase of h_{eq} was smaller than the RC specimen, and the maximum value was 0.26 and was also larger than that of the RC specimen.

The gradient of increase of h_{eq} can be considered in relation with the size of the plastic hinge area mentioned in 3.2. In other words, it is presumed that h_{eq} reflected the fact that the discontinuous area of the longitudinal strain, or the damaged area, was smaller and the amount of energy used there was also smaller in the SRC specimen. Higher energy absorption and damping performance than the RC specimen must eventually be achieved due to the tenacious property unique to synthetic structures.

3.6 Crack behaviors

Figure 11 shows the final crack behavior at the end of experiments of the two specimens and Photograph 4 shows their breaking conditions. It can be seen that the size of the area where concrete exfoliated at the bottom differed greatly between the two specimens.

The exfoliated area at the bottom was obviously larger for the RC specimen. Exfoliation was observed up to approximately 1 m from the bottom and many of the axial rebars were broken.

The exfoliated area at the bottom of the SRC specimen was smaller and was about half that of the RC specimen. Many axial rebars were also broken in the case of the SRC specimen. The exfoliated area almost corresponded with the damaged area mentioned in 3.2.



RC Specimen SRC Specimen
Photo.4 Breaking conditions of specimens

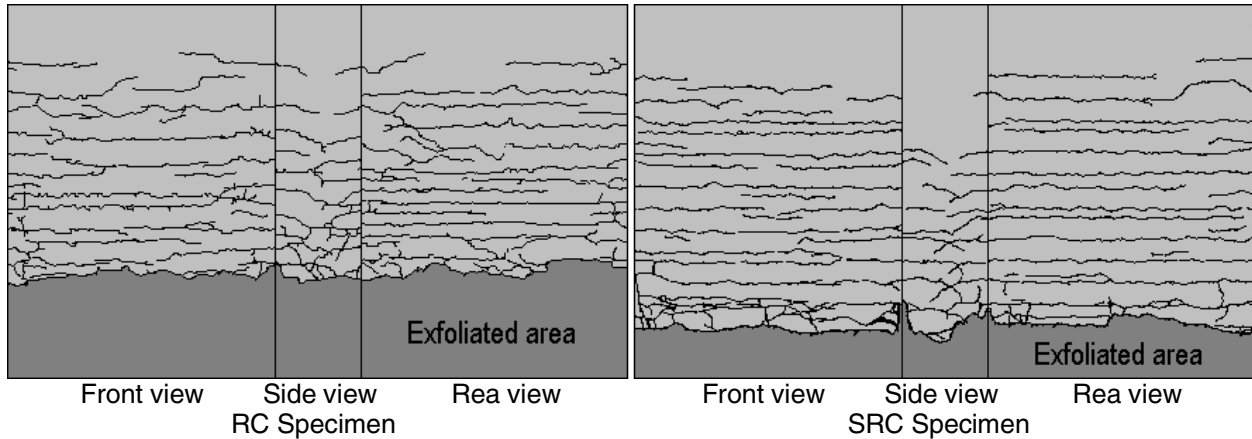


Fig.11 Crack behaviors

4. CONCLUDING REMARKS

A composite bridge pier using steel pipes for which steel pipes with outer ribs were placed instead of axial rebars was proposed as a wall-type pier structure with a large aspect ratio, and its load bearing capacity was studied by the cyclic loading test. The knowledge obtained within the scope of this experiment was as follows:

1. A composite bridge pier using steel pipes has an equal or higher load bearing capacity and toughness compared with a conventional reinforced concrete wall-type pier.
2. Because steel pipes bear a great deal of the shearing force at the bottom of the composite bridge pier incorporating steel pipes, the stress shared by stirrups and tie-bars is small. Damage to the bottom of the pier is thus less than that to a reinforced concrete pier.
3. In the case of a wall-type pier, a composite structure using steel pipes tends to have shorter plastic hinges compared with a reinforced concrete structure. Due to the tenacious property unique to steel pipes, however, a large ductility factor can be maintained and the energy absorption capacity can be equal to or higher than that of a reinforced concrete structure.

REFERENCES

1. Fukumoto E, Kawabata J, Hisa T, Tamura T, Shinozaki H. "Design and construction of steel pipe and concrete composite bridge pier. (ML method)" Bridge and Foundation 1996: 10-15. (In Japanese)
2. Mikami H, Tamura T, Kishi N, Ikeda K. "A study on behaviors of composite bridge pier using steel pipe with outer ribs." Journal of Structural Engineering Vol.47 A, 2001: 1433-44. (In Japanese)
3. Mikami H, Kishi N, Ikeda K, Minakawa M. "An experimental study on toughness of composite bridge piers using steel pipes with outer ribs." Proceedings of the 1st fib Congress 2002 Session 5, 2002: 23-31.
4. Ikeda K, Minakawa M, Mikami H, Kishi N. "Large scale loading tests on steel-pipe with outer-ribs concrete composite wall type pier models." Proceedings of the Japan Concrete Institute Vol.24 No.2 2002: 1591-96. (In Japanese)
5. Minakawa M, Ikeda K, Kishi N, Shinozaki H. "Large scale cyclic and monotonic loading tests on steel-pipe with outer-ribs concrete composite wall type pier models." Proceedings of the Japan Concrete Institute Vol.25 No.2 2003: 1687-92. (In Japanese)
6. Japan road administration "Specification of highway bridge" 2002. (In Japanese)